Adaptive Path Tracking Control for a Four-Mecanum-Wheel Mobile Robot with Unknown Center-of-Gravity Offset and Slope Inclination

Chawannat Chaichumporn[1,2], **Supaluk Prapan**[1], **Nghia Thi Mai**[3], **Md Abdus Samad Kamal**[2], **Iwanori Murakami**[2], and **Kou Yamada**[2†], Non-members

ABSTRACT

This paper proposes a trajectory tracking control framework for a Four-Mecanum-Wheel mobile robot operating on inclined terrain under conditions of dynamic uncertainty. The primary objective is to address the challenge of unknown center-of-gravity offset and unknown slope inclination, which can significantly impact the stability and accuracy of robot motion. To achieve this, a Model Reference Adaptive Control strategy is developed based on a full dynamic model that incorporates the effects of gravity and inertial forces. The proposed controller employs Lyapunov-based adaptation laws to estimate and compensate for uncertain parameters in real time while ensuring asymptotic tracking of a desired trajectory. The simulation results under flat and inclined surface conditions demonstrate the effectiveness of the approach in maintaining tracking performance, regulating control effort, and converging parameter estimates, even when the robot experiences significant changes in center of gravity position and slope terrain.

Keywords: Four-Mecanum-wheel mobile robot, Inclined surface, Center of gravity offset

1. INTRODUCTION

Four-Mecanum-wheel mobile robots (FMWMR) have emerged as a vital class of omnidirectional platforms due to their holonomic mobility, which enables translation in any direction without changing orientation. This characteristic makes them highly suitable for complex tasks in constrained environments such as indoor logistics, warehouse automation, medical robotics, and service operations [1, 2]. Their ability to maneuver precisely in tight spaces gives them a distinct advantage over traditional differential-drive or skid-steering robots.

Most existing control approaches for FMWMR have been based on kinematic models, which are effective for low-speed applications and environments with predictable dynamics [3–5]. These models simplify control design by ignoring dynamic interactions such as inertial forces, gravitational effects, and wheel-ground friction. Although sufficient for basic trajectory tracking, kinematic control alone becomes inadequate when high-performance tracking is required, especially under dynamic or uncertain conditions. To address these challenges, researchers have incorporated dynamic models into control frameworks and applied various strategies such as PID, sliding mode control, and model predictive control (MPC) [6–10].

However, real-world deployment introduces additional complexities, particularly when the center of gravity (CoG) shifts due to payload changes or onboard actuation, and when the robot operates on inclined surfaces. Such conditions significantly alter the dynamic behavior of the system, challenging the accuracy and robustness of conventional controllers. In order to estimate unknown parameters including mass, inertia, and friction in flat-terrain environments, adaptive control methods have been proposed [11–13].

Mobile robots are sometimes used on slopes. The control of mobile robots on slopes has been studied mainly for differential drive platforms, using approaches such as MPC or fuzzy logic [14–18]. Despite these advances, there remains a research gap in the adaptive control of FMWMR on sloped terrain, particularly when both the CoG location and slope angle are unknown and time-varying.

To overcome these limitations, this paper proposes a novel Model Reference Adaptive Control (MRAC) framework specifically designed for FMWMR operating under conditions of unknown CoG offsets and slope inclinations. Unlike previous adaptive control approaches, the proposed method explicitly incorporates a comprehensive dynamic model that simultaneously accounts for both CoG shifts and gravitational effects induced by inclined terrain. The developed controller employs Lyapunov-based adaptive laws to estimate these uncer-

Manuscript received on May 1, 2025; revised on July 7, 2025; accepted on July 18, 2025. This paper was recommended by Associate Editor Matheepot Phattanasak.

[1]The authors are with Faculty of Engineering, Thai-Nichi Institute of Technology, Bangkok, Thailand.

[2]The authors are with Graduate School of Science and Technology, Gunma University, Tenjincho, Kiryu, Japan.

[3]The author is with Faculty of Electronics Engineering 1, Posts and Telecommunications Institute of Technology, Hanoi, Vietnam.

[†]Corresponding author: yamada@gunma-u.ac.jp

Digital Object Identifier: 10.37936/ecti-eec.2525233.258969

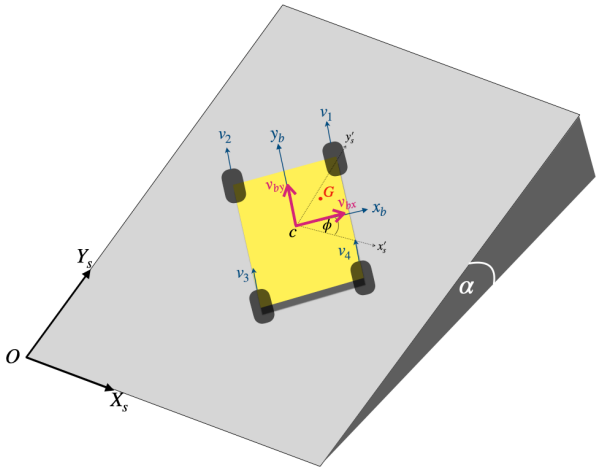

***Fig. 1**: FMWMR operating on sloped terrain. The slope is inclined along the Y_s-axis.*

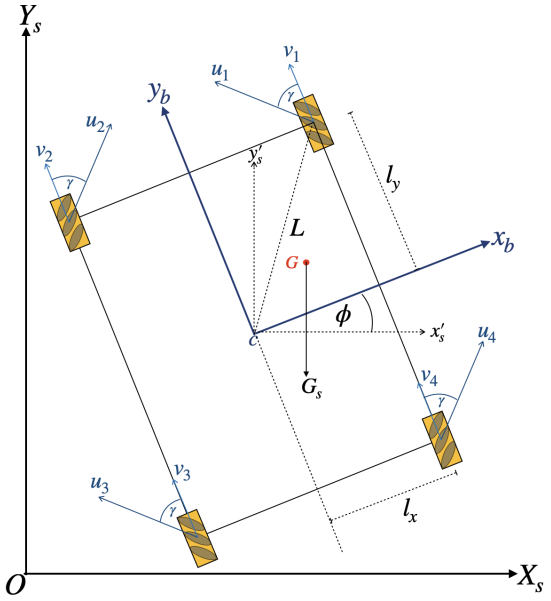

***Fig. 2**: Schematic of the Four-Mecanum-Wheel Mobile Robot (FMWMR), showing the geometric center c, center of gravity G, and wheel arrangement.*

tain parameters in real time [19], guaranteeing not only asymptotic convergence of trajectory tracking but also robustness against dynamic uncertainties. Simulation results demonstrate that the proposed MRAC approach significantly improves tracking accuracy and stability compared to traditional adaptive control methods, particularly under realistic scenarios involving significant CoG offsets and varying slope angles.

This paper is organized as follows. Section 2.explains the system modeling, including both kinematic and dynamic formulations under inclined conditions. Section 3describes the MRAC controller and its adaptive law design. Section 4.provides the stability analysis using Lyapunov's direct method. Section 5.demonstrates the effectiveness of the proposed method through simulations in various terrain and payload conditions. Finally, Section 6concludes the paper and outlines future directions.

2. SYSTEM MODELING

This section explains the modeling framework for the FMWMR operating on inclined terrain. The modeling captures the effect of a shifted CoG and the gravitational force acting along the slope.

The concept of the CoG offset and its impact on the kinematics is first described. Then, the dynamic equations are derived using the Newton-Euler formulation with respect to the CoG frame and subsequently transformed to the geometric center.

Consider the FMWMR operating on an inclined plane, as illustrated in Fig. 1. The global coordinate system is defined as $\{X_s, O, Y_s\}$, with the slope inclined at an angle α relative to the ground, tilted about the Y_s-axis. The robot's state in the global frame is described by the pose vector $\boldsymbol{q} = [x, y, \phi]^{\mathrm{T}}$, where x and y denote the coordinates of the geometric center c, and ϕ is the yaw angle. This yaw angle ϕ is defined as the angle between the robot's body-frame x_b-axis and the rotated global axis x_s' projected onto the inclined plane.

The robot's local body frame is denoted by $\{x_b, c, y_b\}$, with its forward direction aligned along the positive y_b-axis. The robot's velocity in the body frame is represented by $\boldsymbol{v_b} = [v_{bx}, v_{by}, \omega_{b\phi}]^{\mathrm{T}}$, which includes the linear velocity components along the x_b and y_b axes, as well as the angular velocity about the vertical axis. The CoG point $\boldsymbol{G}$ is offset from the geometric center c by the coordinates (x_g, y_g), expressed in the body frame.

The schematic diagram of the FMWMR, shown in Fig. 2, illustrates the key geometric parameters of the system. The quantities l_x and l_y denote half of the robot's width and length, respectively, measured from the geometric center c. The distance from the geometric center to each wheel is represented by L. Each Mecanum wheel is equipped with rollers mounted at an angle γ, typically set to $\pi/4$ [rad] relative to the wheel axis, to enable omnidirectional motion. The linear velocity and traction force acting on the i-th wheel are denoted by v_i and u_i, respectively, for $i = 1, 2, 3, 4$. The gravitational force vector acting in the slope frame is indicated by G_s. Together, these parameters define the geometric layout and influence the dynamic behavior of the FMWMR when operating on inclined terrain.

2.1 Kinematic Model

The velocity of the geometric center in the global frame, denoted by $\dot{\boldsymbol{q}} = [\dot{x}, \dot{y}, \dot{\phi}]^{\mathrm{T}}$, is related to the body-frame velocity $\boldsymbol{v_b}$ through a standard rotation transformation. This transformation accounts for the robot's orientation in the plane, ensuring that velocities are properly represented in the global reference frame.

The relationship is given by:

$$\dot{\boldsymbol{q}} = \boldsymbol{R}(\boldsymbol{\phi})\boldsymbol{v_b}, \tag{1}$$

where $\boldsymbol{R}(\boldsymbol{\phi})$ is the rotation matrix that transforms body-frame velocities to the global frame, defined as:

$$\boldsymbol{R}(\boldsymbol{\phi}) = \begin{bmatrix} \cos\phi & -\sin\phi & 0 \\ \sin\phi & \cos\phi & 0 \\ 0 & 0 & 1 \end{bmatrix}.$$

This transformation is fundamental for trajectory tracking, as it ensures that velocity commands generated in the robot's body frame result in the desired motion in the global coordinate system.

2.2 Dynamic Model

To facilitate control design that accounts for realistic dynamic effects on inclined terrain, a full-body-frame dynamic model is derived using the Newton–Euler formulation. In this modeling approach, several assumptions are adopted. Wheel slip is neglected to ensure perfect rolling contact, CoG is permitted to be offset from the geometric center due to potential payload shifts, and the terrain is assumed to be inclined at an unknown angle, introducing gravity components along the slope. The equations of motion are initially formulated in the robot's body frame with the origin located at the CoG. To simplify the model for control purposes, these equations are subsequently transformed to the geometric center, which serves as the reference point for planning and control. The resulting dynamic model in the body frame is expressed as:

$$\boldsymbol{H}\dot{\boldsymbol{v}}_{\boldsymbol{b}} + \boldsymbol{C}\boldsymbol{v}_{\boldsymbol{b}} + \boldsymbol{G}_{\boldsymbol{b}} = \boldsymbol{F}_{\boldsymbol{\tau}}, \tag{2}$$

where $\boldsymbol{H}$ denotes the constant inertia matrix at the geometric center, $\boldsymbol{C}$ is the Coriolis and centrifugal matrix, and $\boldsymbol{G}_{\boldsymbol{b}}$ represents the gravitational force vector projected into the body frame. The wheel configuration matrix, which maps wheel forces to body-frame forces and torque, is denoted by $\boldsymbol{B}$. The vector $\boldsymbol{F}_{\boldsymbol{\tau}}$ represents the resulting control force in the body frame.

The inertia matrix is defined as:

$$\boldsymbol{H} = \begin{bmatrix} m & 0 & -my_g \\ 0 & m & mx_g \\ -my_g & mx_g & I_z \end{bmatrix},$$

where m is the mass of the robot and I_z is moment of inertia of rotation.

The Coriolis and centrifugal matrix is expressed as:

$$\boldsymbol{C} = \begin{bmatrix} 0 & -m\omega_{b\phi} & -m\omega_{b\phi}y_g \\ m\omega_{b\phi} & 0 & m\omega_{b\phi}x_g \\ m\omega_{b\phi}y_g & -m\omega_{b\phi}x_g & 0 \end{bmatrix}.$$

The gravitational force vector in the global frame $\boldsymbol{G}_{\boldsymbol{s}} = [0, mg\sin\alpha, 0]^{\mathrm{T}}$, is transformed into the body frame as:

$$\boldsymbol{G}_{\boldsymbol{b}} = mg\sin\alpha \begin{bmatrix} \sin\phi \\ \cos\phi \\ x_g\cos\phi - y_g\sin\phi \end{bmatrix}.$$

The vector of traction force in the body frame, denoted by F_τ, represents the net force and torque generated by the wheels. It is given by:

$$\boldsymbol{F}_{\boldsymbol{\tau}} = \boldsymbol{B}\boldsymbol{u}_{\boldsymbol{s}}, \tag{3}$$

where $\boldsymbol{u}_{\boldsymbol{s}} = [u_{s,1}, u_{s,2}, u_{s,3}, u_{s,4}]^{\mathrm{T}}$ is the vector of individual wheel forces after applying saturation. Each component $u_{s,i}$ corresponds to the traction force command of the i-th wheel, ensuring that it remains within the allowable friction limit described in the next subsection. The configuration matrix $\boldsymbol{B}$ maps the individual wheel forces to the resulting body-frame forces and torque, and is defined as:

$$\boldsymbol{B} = \frac{1}{\sqrt{2}} \begin{bmatrix} -1 & 1 & -1 & 1 \\ 1 & 1 & 1 & 1 \\ L\sqrt{2} & -L\sqrt{2} & -L\sqrt{2} & L\sqrt{2} \end{bmatrix}.$$

2.3 Maximum Friction Force

In real-world scenarios, the traction force that each wheel can exert is fundamentally limited by the static friction available between the wheel and the ground. Exceeding this limit results in wheel slip, which can significantly reduce tracking accuracy and even lead to instability, issues that are particularly pronounced on inclined terrain.

To ensure a physically realistic and safe operation, the control design incorporates Coulomb friction constraints on the commanded wheel forces. The maximum static friction force that can be generated by the i-th wheel is modeled as:

$$F_{f,\max,i} = \mu N_i, \tag{4}$$

where μ denotes the static coefficient of friction between the wheel and the ground, and N_i represents the normal force acting on wheel i. This normal force is not uniform but varies with the robot's weight distribution, the slope inclination, and the CoG offset.

The distribution of normal forces captures how the robot's load dynamically shifts across the wheels, directly affecting their traction capacity. This effect is systematically modeled as:

$$\begin{aligned} N_1 &= \frac{mg\cos\alpha}{4}\left(1 + \frac{x_g}{l_x} + \frac{y_g}{l_y}\right), \\ N_2 &= \frac{mg\cos\alpha}{4}\left(1 - \frac{x_g}{l_x} + \frac{y_g}{l_y}\right), \\ N_3 &= \frac{mg\cos\alpha}{4}\left(1 - \frac{x_g}{l_x} - \frac{y_g}{l_y}\right), \\ N_4 &= \frac{mg\cos\alpha}{4}\left(1 + \frac{x_g}{l_x} - \frac{y_g}{l_y}\right). \end{aligned}$$

To respect these physical constraints in control execution, a component-wise saturation function is applied:

$$u_{s,i} = \mathrm{sat}(u_i, \pm F_{f,\max,i}), \tag{5}$$

which enforces that each wheel command u_i remains bounded within $\pm F_{f,\max,i}$. This saturation ensures that the controller never requests wheel forces beyond what physical contact with the ground can transmit. By enforcing this limit, the controller guarantees physically consistent actuation, prevents slip, and enhances the reliability of path tracking even when the robot experiences variations in payload distribution or operates on sloped surfaces. This approach is essential to achieve robust and safe motion in real-world deployments.

3. ADAPTIVE CONTROLLER DESIGN

MRAC strategy is proposed for the FMWMR, addressing uncertainties in mass, CoG offset, and slope inclination. The control design is formulated based on the body-frame dynamic model to ensure robust trajectory tracking performance under these unknown parameters.

3.1 Filtered Tracking Error Formulation

The control objective is to ensure that the robot's pose q_c tracks the desired trajectory $\boldsymbol{q_d} = [x_d, y_d, \phi_d]^{\mathrm{T}}$. The tracking error is defined as $\tilde{\boldsymbol{q}} = \boldsymbol{q} - \boldsymbol{q_d}$. To facilitate the controller design, the reference velocity is introduced as $\dot{\boldsymbol{q}}_{\boldsymbol{r}} = \dot{\boldsymbol{q}}_{\boldsymbol{d}} - \lambda\tilde{\boldsymbol{q}}$, where λ is a positive-definite gain matrix that determines the convergence rate of the tracking error.

The filtered tracking error represents the velocity error expressed in the body frame and is defined as:

$$\boldsymbol{s} = \boldsymbol{v_b} - \boldsymbol{v_r}, \tag{6}$$

where $\boldsymbol{v_r} = \boldsymbol{R}(\phi)^{\mathrm{T}}\dot{\boldsymbol{q}}_{\boldsymbol{r}}$ is the reference velocity transformed into the body frame using the rotation matrix $\boldsymbol{R}(\phi)$. Its time derivative is given by $\dot{\boldsymbol{s}} = \dot{\boldsymbol{v}}_{\boldsymbol{b}} - \dot{\boldsymbol{v}}_{\boldsymbol{r}}$, capturing the difference between actual and reference accelerations. Combining the definition of filtered error with the body-frame dynamic model in (2) yields:

$$\boldsymbol{H}\dot{\boldsymbol{s}} + \boldsymbol{C}\boldsymbol{v_b} + \boldsymbol{G_b} = \boldsymbol{B}\boldsymbol{u} - \boldsymbol{H}\dot{\boldsymbol{v}}_{\boldsymbol{r}}. \tag{7}$$

By substituting $\boldsymbol{v_b}$ from (6) into (7) and rearranging terms involving reference velocity on the right-hand side, the error dynamics are expressed as:

$$\boldsymbol{H}\dot{\boldsymbol{s}} + \boldsymbol{C}\boldsymbol{s} = \boldsymbol{B}\boldsymbol{u} - \left(\boldsymbol{H}\dot{\boldsymbol{v}}_{\boldsymbol{r}} + \boldsymbol{C}\boldsymbol{v_r} + \boldsymbol{G_b}\right). \tag{8}$$

3.2 Parameterization of the Dynamic Model

The core of MRAC is to linearly parameterize the uncertain dynamics. The term in the parenthesis in (8) contains all the dynamic terms and can be written as a product of a known regressor matrix $\boldsymbol{Y}$ and an unknown parameter vector $\boldsymbol{\theta}$.

$$\boldsymbol{Y}\boldsymbol{\theta} = \boldsymbol{H}\dot{\boldsymbol{v}}_{\boldsymbol{r}} + \boldsymbol{C}\boldsymbol{v_r} + \boldsymbol{G_b}. \tag{9}$$

The vector $\boldsymbol{\theta}$ is the unknown parameter vector to be estimated defined by:

$$\boldsymbol{\theta} = [\theta_1, \theta_2, \theta_3, \theta_4, \theta_5, \theta_6, \theta_7]^{\mathrm{T}},$$

where $\theta_1 = m$, $\theta_2 = I_z$, $\theta_3 = mx_g$, $\theta_4 = my_g$, $\theta_5 = m\sin\alpha$, $\theta_6 = mx_g\sin\alpha$, $\theta_7 = my_g\sin\alpha$.

The regressor matrix $\boldsymbol{Y}$ is constructed from known reference signals, including the reference velocities $\boldsymbol{v_r}$, their derivatives $\dot{\boldsymbol{v}}_{\boldsymbol{r}}$, and the measured orientation ϕ. Let $\boldsymbol{v_r} = [v_{rx}, v_{ry}, \omega_{r\phi}]^{\mathrm{T}}$. The matrix $\boldsymbol{Y}$ is defined as a 3×7 regressor that captures the relationship between these signals and the system dynamics and is expressed as:

$$\boldsymbol{Y} = \begin{bmatrix} y_{11} & y_{12} & 0 \\ 0 & 0 & \dot{\omega}_{r\phi} \\ 0 & y_{23} & y_{33} \\ y_{14} & 0 & y_{34} \\ g\cos\phi & g\sin\phi & 0 \\ 0 & 0 & g\cos\phi \\ 0 & 0 & -g\sin\phi \end{bmatrix}^{\mathrm{T}},$$

where the components are defined as:

$$\begin{aligned} y_{11} &= \dot{v}_{rx} - v_{ry}\omega_{r\phi}, & y_{12} &= \dot{v}_{ry} - v_{rx}\omega_{r\phi}, \\ y_{23} &= \dot{\omega}_{r\phi} + \omega_{r\phi}^2, & y_{33} &= \dot{v}_{ry} + v_{ry}\omega_{r\phi}, \\ y_{14} &= -(\dot{\omega}_{r\phi} + \omega_{r\phi}^2), & y_{34} &= -(\dot{v}_{rx} + v_{rx}\omega_{r\phi}). \end{aligned}$$

Since the parameter vector $\boldsymbol{\theta}$ in (9) is unknown, it must be estimated. The method for estimating is described in the following subsection.

3.3 Control Law and Adaptive Update Rule

With the dynamic model now represented in a linearly parameterized form, a control law and an adaptive update rule are designed to leverage this structure. The control input is computed using the regressor matrix and the current estimates of the unknown parameters to minimize tracking error. Simultaneously, the adaptive law continuously updates the parameter estimates in real time to enhance tracking performance.

Since $\boldsymbol{\theta}$ is unknown, an estimated parameter $\hat{\boldsymbol{\theta}}$ is employed in its place. To address uncertainties in the system parameters and ensure accurate trajectory tracking, the control input is formulated as

$$\boldsymbol{u} = \boldsymbol{B}^{\mathrm{T}}(\boldsymbol{B}\boldsymbol{B}^{\mathrm{T}})^{-1}\left(\boldsymbol{Y}\hat{\boldsymbol{\theta}} - \boldsymbol{K}\boldsymbol{s}\right), \tag{10}$$

where $\boldsymbol{K}$ is a symmetric positive-definite matrix for reducing the tracking error, and $\hat{\boldsymbol{\theta}}$ is the current estimate of the unknown parameter vector. The adaptation law for updating the parameter estimates is chosen as:

$$\dot{\hat{\boldsymbol{\theta}}} = -\boldsymbol{\Gamma}\boldsymbol{Y}^{\mathrm{T}}\boldsymbol{s}, \tag{11}$$

where $\boldsymbol{\Gamma}$ is a symmetric positive-definite adaptation gain matrix.

3.4 Control Architecture Overview

The control architecture of the proposed MRAC framework is illustrated in Fig.3. The reference block provides the desired trajectory in terms of position, velocity, and acceleration. These are compared with

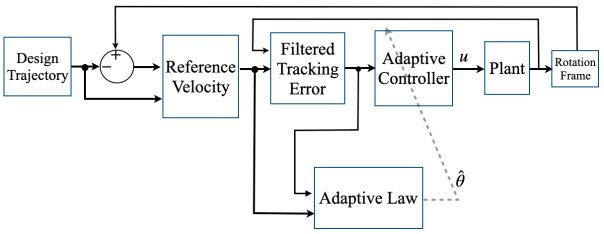

***Fig. 3**: Block diagram of the proposed Model Reference Adaptive Control framework.*

the actual states of the plant to compute the tracking error. This error is fed into the reference velocity block, which applies a stabilizing filter to produce the reference velocity signal used for control design. The Filtered Tracking Error block then calculates the filtered error as defined in (6), capturing the difference between actual and reference velocities in the body frame, which is then fed into both the Adaptive Controller (10) and the Adaptive Law (11). The adaptive controller generates the control input u based on the current estimate of the dynamic parameters $\hat{\theta}$, which are continuously updated by the adaptive law using a gradient-based update rule. The plant (2) receives the control input and responds accordingly, with its output states fed back into the loop. This closed-loop structure ensures that the robot follows the reference trajectory while adapting to parametric uncertainties in real time.

4. LYAPUNOV-BASED STABILITY

To verify the stability of the proposed adaptive control system, the closed-loop dynamics is analyzed using the Lyapunov direct method. The objective is to ensure that the tracking error converges asymptotically to zero, even in the presence of parametric uncertainties.

The Lyapunov candidate function is first defined as follows:

$$V = \frac{1}{2}\boldsymbol{s}^{\mathrm{T}}\boldsymbol{H}\boldsymbol{s} + \frac{1}{2}\tilde{\boldsymbol{\theta}}^{\mathrm{T}}\boldsymbol{\Gamma}^{-1}\tilde{\boldsymbol{\theta}}, \tag{12}$$

where $\tilde{\boldsymbol{\theta}} = \hat{\boldsymbol{\theta}} - \boldsymbol{\theta}$ represents the parameter estimation error. Since the unknown parameter vector θ is assumed to be constant, it follows that $\dot{\tilde{\boldsymbol{\theta}}} = \dot{\hat{\boldsymbol{\theta}}}$. By taking the time derivative of equation (12), the following expression is obtained:

$$\dot{V} = \boldsymbol{s}^{\mathrm{T}}\boldsymbol{H}\dot{\boldsymbol{s}} + \frac{1}{2}\boldsymbol{s}^{\mathrm{T}}\dot{\boldsymbol{H}}\boldsymbol{s} + \tilde{\boldsymbol{\theta}}^{\mathrm{T}}\boldsymbol{\Gamma}^{-1}\dot{\hat{\boldsymbol{\theta}}}. \tag{13}$$

Next, the time derivative of the Lyapunov function in (13) is simplified by substituting the filtered tracking error (6) and the system dynamics (2), and by rearranging the resulting terms, an intermediate expression for the Lyapunov derivative is obtained. The term $\boldsymbol{s}^{\mathrm{T}}(1/2\dot{\boldsymbol{H}} - \boldsymbol{C})\boldsymbol{s}$ vanishes due to the skew-symmetric property of $\dot{\boldsymbol{H}} - 2\boldsymbol{C}$. Substituting the linear parameterization of the dynamics using the regressor matrix and the parameter vector as defined in equation (9), the Lyapunov derivative simplifies to

$$\dot{V} = \boldsymbol{s}^{\mathrm{T}}(\boldsymbol{B}\boldsymbol{u} - \boldsymbol{Y}\boldsymbol{\theta}) + \tilde{\boldsymbol{\theta}}^{\mathrm{T}}\boldsymbol{\Gamma}^{-1}\dot{\hat{\boldsymbol{\theta}}}. \tag{14}$$

By substituting the control input u in (10) and the adaptation law in (11) into the simplified Lyapunov derivative in (14), the following result is obtained:

$$\dot{V} = -\boldsymbol{s}^{\mathrm{T}}\boldsymbol{K}\boldsymbol{s}.$$

Since $\boldsymbol{K}$ is a symmetric positive-definite matrix, it follows that $\dot{V} \leq 0$ for all s, which implies that the closed-loop system is Lyapunov stable. Furthermore, because V is positive definite and $\dot{V}$ is negative semi-definite, all signals in the system remain bounded. By applying Barbalat's Lemma, it is concluded that $\boldsymbol{s}(t) \to 0$ as $t \to \infty$, guaranteeing the asymptotic convergence of both position and velocity tracking errors. This confirms the effectiveness and robustness of the proposed adaptive control strategy in the presence of parameter uncertainties.

5. SIMULATION RESULTS

This section shows the simulation studies conducted to evaluate the performance of the proposed adaptive controller for an FMWMR operating on an inclined surface. The simulation demonstrates the controller's ability to follow a reference trajectory with parametric uncertainties that include unknown mass, CoG offset, and slope inclination. All simulations are performed using MATLAB/Simulink.

5.1 Simulation Setup

The physical parameters of the robot used in the simulation are specified as follows The total mass of FMWMR is set to $m = 20$ [kg]. The half-width and half-length are $l_x = 0.4$ [m] and $l_y = 0.6$ [m], respectively. The moment of inertia on the vertical axis is $I_z = 3.46$ [kg $\cdot$ m^2]. The gravitational acceleration is set to $g = 9.81$ [m/s^2]. The static coefficient of friction between the wheels and the ground is assumed to be $\mu = 1$.

5.2 Reference Trajectory Design

To evaluate the tracking performance of the proposed control system, a simple time-varying desired trajectory is defined. The desired positions in both the x- and y-directions are defined as parabolic functions of time, resulting in constant acceleration and linearly increasing velocity profiles. The robot is required to start from rest at the origin and track the desired trajectory with both translational and rotational alignment.

The desired trajectory is defined as:

$$x_d(t) = y_d(t) = 2 + 0.01t^2 \text{ [m]},$$

$$\dot{x}_d(t) = \dot{y}_d(t) = 0.02t \text{ [m/s]},$$

$$\ddot{x}_d(t) = \ddot{y}_d(t) = 0.02 \text{ [m/s}^2\text{]}.$$

The robot is initialized at the position $x = 0$ [m], $y = 0$ [m] with a heading angle aligned with the positive y-axis. The desired orientation is set to remain constant throughout the trajectory, with an initial and target value of $\phi_d = 0$ [rad]. This setup ensures that the robot must not only follow the translational path but also maintain its heading direction consistent with the initial alignment.

5.3 Results and Analysis

The simulation is conducted for two distinct scenarios. In the first case, the robot operates on a flat surface with the CoG located at the geometric center of the robot. In the second case, the robot operates on a sloped surface tilted about the global y-axis with an angle of $\alpha = \pi/18$ [rad], and the CoG is shifted to a position offset by $x_g = 0.1$ [m] and $y_g = 0.1$ [m], placing it in the first quadrant of the robot frame.

For both scenarios, the adaptive controller is applied using manually tuned gain parameters to ensure smooth trajectory tracking. The controller gains are set as $\boldsymbol{\lambda} = \text{diag}[0.4, 0.4, 0.4]$, $\boldsymbol{K} = \text{diag}[80, 80, 80]$, $\boldsymbol{\Gamma} = \text{diag}[2.5, 10, 10, 10, 0.25, 0.5, 0.5]$. These values were chosen to balance adaptation speed with parameter convergence stability, ensuring numerical stability in simulation without excessive oscillation. If the initial condition is changed, the same gains are still used as in this test.

Figs. 4 and 5 present the simulation results for two scenarios: a flat surface with a centralized CoG and an inclined surface with an offset CoG. In these graphs, the labels x-design, y-design, and ϕ-design indicate the desired trajectories in the x, y, and yaw (ϕ) directions, while x-actual, y-actual, and ϕ-actual denote the actual measured responses of the robot under control.

Fig. 4 illustrates the tracking performance of the robot operating on a flat surface with the CoG located at the geometric center. Fig. 4(a) and (b) show the position tracking in the x- and y-directions, respectively. The robot successfully follows the desired parabolic trajectory with minimal deviation, converging to the planned path within approximately 10 seconds. This behavior confirms that the proposed controller effectively compensates for dynamic effects even in acceleration phases. Fig. 4(c) displays the yaw angle ϕ, demonstrating that the robot maintains a constant heading aligned with the global y-axis throughout the maneuver. This alignment is crucial for ensuring stable trajectory tracking and validates the controller's ability to regulate orientation under dynamic conditions. Fig. 4(d) presents the tracking errors in the x- and y-directions, both of which converge steadily to zero at similar rates, demonstrating balanced and coordinated control action in the translational axes. Additionally, the yaw error ϕ remains small throughout the motion, confirming the controller's ability to maintain a stable and precise heading while ensuring smooth overall trajectory tracking. Fig. 4(e) shows the traction forces applied to each wheel, which remain smooth and

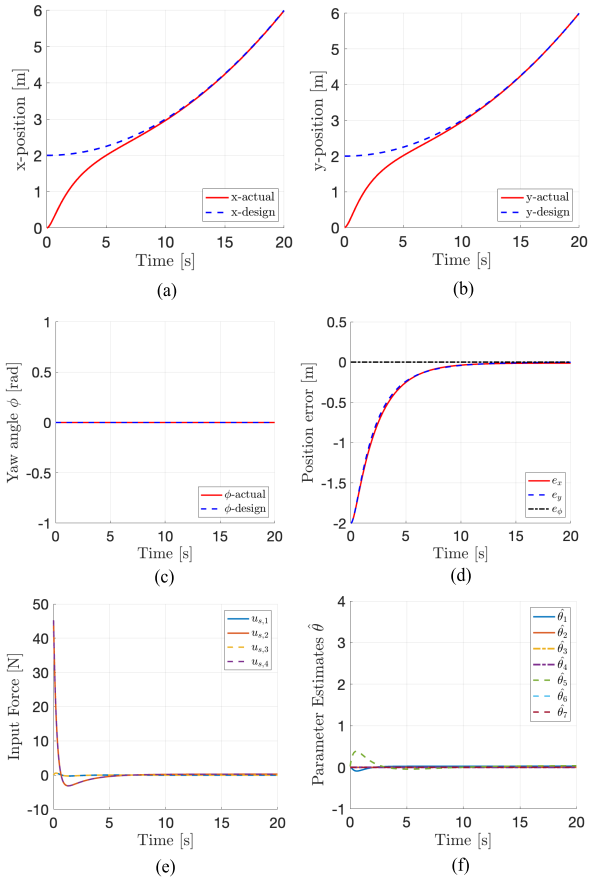

***Fig. 4**: Tracking results under flat surface condition with CoG located at the geometric center. Trajectory position tracking in global frame: (a) $x(t)$, (b) $y(t)$, (c) Orientation $\phi(t)$, (d) Position tracking error, (e) Control input and (f) Parameter estimation $\hat{\theta}(t)$.*

well bounded without any excessive oscillation. The commanded diagonal trajectory at $\pi/4$ [rad] relative to the x-axis requires wheels 2 and 4 to generate significantly higher and balanced traction forces compared to wheels 1 and 3. The simulation results closely match this expected distribution, with a peak traction force of approximately 45 [N] observed during the initial acceleration phase. This agreement between prediction and simulation reinforces the accuracy of the dynamic model and control allocation strategy. Finally, Fig. 4(f) illustrates the time evolution of the estimated parameters $\hat{\theta}(t)$. The adaptive controller effectively updates these estimates online, exhibiting stable convergence behavior. This adaptive mechanism ensures that the tracking error converges to zero despite dynamic changes, confirming the robustness and learning capability of the proposed control law under nominal flat-surface conditions with a centered CoG.

Fig. 5 shows the simulation results for the second scenario, where the robot operates on a sloped surface inclined at $\alpha = \pi/18$ [rad] about the global y-axis. The CoG is deliberately shifted from the geometric center

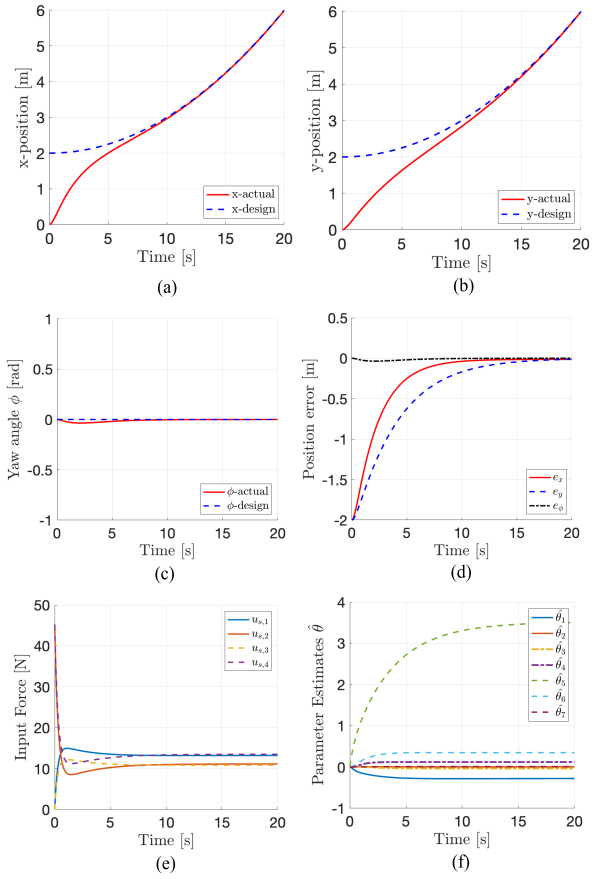

***Fig. 5**: Tracking results under sloped surface with shifted CoG. Trajectory position tracking in global frame: (a) $x(t)$, (b) $y(t)$, (c) Orientation $\phi(t)$, (d) Position tracking error, (e) Control input and (f) Parameter estimation $\hat{\theta}(t)$.*

to $x_g = 0.1$ [m] and $y_g = 0.1$ [m], introducing a realistic challenge that tests the controller's robustness. Despite these disturbances, the robot is commanded to follow the same desired parabolic trajectory while initially facing along the positive y-axis. Fig. 5(a) and (b) show the position tracking in the x- and y-directions, respectively. The trajectory in the x-direction converges to the desired path within approximately 10 seconds, while the y-direction requires around 15 seconds due to gravitational components acting along the slope. Nevertheless, both axes ultimately achieve minimal steady-state deviation, confirming the controller's ability to compensate for slope-induced disturbances. Fig. 5(c) presents the yaw orientation $\phi(t)$. The CoG offset in the first quadrant of the robot's frame induces a transient clockwise torque about the z-axis. The adaptive controller effectively counters this disturbance, maintaining a stable and accurate heading throughout the maneuver. This demonstrates the controller's ability to manage rotational dynamics even under non-ideal conditions. Fig. 5(d) illustrates the tracking errors in the x- and y-directions as well as the rotational error about the z-axis. The x-error converges more quickly than the y-error due to the directional component of gravity along the slope, while the small transient rotational error is rapidly corrected. These error profiles validate the controller's capacity for anisotropic adaptation, prioritizing response along more disturbed directions. Fig. 5(e) shows the traction forces applied to each wheel as the robot tracks a diagonal trajectory at $\pi/4$ relative to the x-axis. Combined disturbances from the inclined surface and the CoG offset introduce an undesired clockwise moment about the z-axis. The control system compensates by applying greater traction force to wheel 4 than to wheel 2, demonstrating intelligent force allocation to maintain accurate heading and trajectory. This behavior confirms that the control allocation strategy can handle complex interactions between slope and mass distribution. Finally, Fig. 5(f) shows the evolution of the parameter estimates. The adaptive law accurately updates these estimates in real time, ensuring convergence of the tracking errors despite the challenging terrain and CoG offset. This result confirms the robustness and learning capability of the proposed adaptive control system, even in the presence of significant modeling uncertainties.

6. CONCLUSION

This paper has proposed a MRAC strategy to track the trajectory of a FMWMR subject to uncertainties in the position of the CoG and the unknown slope inclination. The objective is to enable robust path-following control in realistic environments where the dynamic parameters of the robot are not precisely known. To this end, a dynamic model incorporating CoG offset and gravitational effects is used to derive a regressor-based control law, coupled with Lyapunov-based adaptation to ensure closed-loop stability. Simulation results validated the controller's performance in two representative scenarios: motion on a flat surface with centralized CoG, and motion on a sloped surface with an offset CoG. In both cases, the adaptive controller achieved smooth trajectory tracking, accurate parameter estimation, and bounded control input. These results confirm the feasibility of the proposed MRAC framework for adaptive compensation of parametric uncertainties in real-time robotic applications.

Future work will include experimental implementation, consideration of external disturbances such as payload shifts and wheel slip, and extension of the control strategy to 3D terrain environments.

ACKNOWLEDGMENT

The authors would like to thank the research and development team of the Thai-Nichi Institute of Technology and Gunma University for providing the infrastructure and collaboration opportunities that made this study possible. This work is partially supported by JSPS KAKENHI Grant Number JP21K03930.

REFERENCES

[1] S. L. Dickerson and B. D. Lapin, "Control of an omni-directional robotic vehicle with Mecanum wheels," in *Proceedings of the National Telesystems Conference (NTC)*, Atlanta, GA, USA, 1991, pp. 323–328.

[2] A. Gfrerrer, "Geometry and kinematics of the Mecanum wheel," *Computer Aided Geometric Design*, vol. 25, no. 9, pp. 784–791, Nov. 2008.

[3] S. G. Tzafestas. *Introduction to Mobile Robot Control*. Amsterdam: Elsevier, 2013.

[4] G. Klancar, A. Zdesar, S. Blazic, and I. Skrjanc. *Wheeled Mobile Robotics: From Fundamentals Towards Autonomous Systems*. Oxford: Butterworth-Heinemann, 2017.

[5] Z. Hendzel and L. Rykala, "Modelling of dynamics of a wheeled mobile robot with Mecanum wheels with the use of Lagrange equations of the second kind," *International Journal of Applied Mechanics and Engineering*, vol. 22, no. 1, 2017, pp. 81–99.

[6] X. Lu, X. Zhang, G. Zhang, and S. Jia, "Design of adaptive sliding mode controller for four-Mecanum wheel mobile robot," in *Proceedings of the 37th Chinese Control Conference (CCC)*, Wuhan, China, 2018, pp. 3983–3987.

[7] I. Zeidis and K. Zimmermann, "Dynamics of a four-wheeled mobile robot with Mecanum wheels," *ZAMM - Journal of Applied Mathematics and Mechanics*, vol. 99, no. 12, Dec. 2019.

[8] H. Zorski, "Fundamentals of mechanics," in *Foundations of Mechanics*, vol. 28, Amsterdam: Elsevier, 1992, pp. 49–81.

[9] I. Moreno-Caireta, E. Celaya, and L. Ros, "Model predictive control for a Mecanum-wheeled robot navigating among obstacles," *IFAC-PapersOnLine*, vol. 54, no. 6, pp. 119–125, 2021.

[10] V. Alakshendra and S. Chiddarwar, "Adaptive robust control of Mecanum-wheeled mobile robot with uncertainties," *Nonlinear Dynamics*, vol. 87, pp. 2147–2169, 2017.

[11] Y. N. Wang et al., "Adaptive control method for a walking support machine considering center-of-gravity shifts and load changes," in *Proceedings of the International Conference on Advanced Mechatronic Systems*, Tokyo, Japan, 2012, pp. 684–689.

[12] R. Tan, S. Wang, Y. Jiang, K. Ishida, and M. G. Fujie, "Adaptive control of an omni-directional walker considering the forces caused by user," in *Proceedings of the IEEE International Conference on Mechatronics and Automation (ICMA)*, Takamatsu, Japan, 2013, pp. 761–766.

[13] K. Kawamura, T. Emaru, Y. Kobayashi, and A. A. Ravankar, "Adaptive control for omnidirectional wheeled robot," in *Proceedings of the IEEE/SICE International Symposium on System Integration (SII)*, Sapporo, Japan, 2016, pp. 367–372.

[14] S. O. Onyango, Y. Hamam, K. Djouani, and G. Qi, "Dynamic control of powered wheelchair with slip on an incline," in *Proceedings of the 2nd International Conference on Adaptive Science and Technology (ICAST)*, Accra, Ghana, 2009, pp. 278–283.

[15] H. Qi, J. Shangguan, C. Fang, and M. Yue, "Path tracking control of car-like wheeled mobile robot on the slope based on nonlinear model predictive control," in *Proceedings of the International Conference on Advanced Robotics and Mechatronics (ICARM)*, Guilin, China, 2022, pp. 465–470.

[16] X. Yue, J. Chen, Y. Li, et al., "Path tracking control of skid-steered mobile robot on the slope based on fuzzy system and model predictive control," *International Journal of Control, Automation and Systems*, vol. 20, pp. 1365–1376, Oct. 2022.

[17] H. B. Santos et al., "Model predictive torque control for velocity tracking of a four-wheeled climbing robot," *Sensors*, vol. 20, no. 24, p. 7059, Dec. 2020.

[18] C. Chaichumporn et al., "The Dynamical Modeling of Four Mecanum Wheel Mobile Robot on Typical Unstructured Terrain," in *Proceedings of the 21st International Conference on Electrical Engineering/Electronics, Computer, Telecommunications and Information Technology (ECTI-CON)*, Khon Kaen, Thailand, 2024, pp. 1–5.

[19] J.-J. E. Slotine and W. Li. *Applied Nonlinear Control*, 1st ed. Englewood Cliffs, NJ: Prentice Hall, 1991.

Chawannat Chaichumporn received the B.Sc. degree in Electronics Physics in 2009 and the M.Sc. degree in Physics in 2014, both from Thammasat University, Thailand. Since 2016, he has been serving as a lecturer in the Faculty of Engineering at the Thai-Nichi Institute of Technology (TNI), Thailand. His research interests include control systems for mobile robotic platforms.

Supaluk Prapan received B.Sc. and M.Sc. degrees in Physics from King Mongkut's University of Technology Thonburi, Thailand, in 2007 and 2011, respectively. Since 2012, She has been serving as a lecturer in the Faculty of Engineering at the Thai-Nichi Institute of Technology (TNI), Thailand. Her research interests include mechanical physics and nanomaterials.

Nghia Thi Mai received the B.S., M.S and Dr. Eng. degrees from Gunma University, Gunma, Japan in 2009, 2011 and 2014, respectively. From 2014 to 2015, she was with the Human Resources Cultivation Center, Gunma University, Gunma, Japan as a research associate. From 2015 to 2021, she worked on research on damping control for automobiles at Exedy Co., Ltd. Since 2022, she have been working as a lecturer at the Faculty of Electrical and Electronic 1, Posts and Telecommunications Institute of Technology (PTIT). In addition, she is currently working as a visiting associate professor and part-time lecturer at the Faculty of Electronics and Mechanical Engineering, Gunma University. Her research interest includes Smith predictor, Internal Model Control and Robotics.

Md Abdus Samad Kamal received the B.Sc. degree in Electrical and Electronic Engineering from Khulna University of Engineering and Technology (KUET), Khulna, Bangladesh in 1997; Master and Doctor degrees from Kyushu University from Graduate School of Information Science and Electrical Engineering, Japan in 2003 and 2006, respectively. He was a post-doctoral fellow in Kyushu University till November 2006.
Dr. Kamal is currently a full-time associate professor at Faculty of Science and Technology, Gunma University, Japan. His current research interests are reinforcement learning, intelligent transportation systems, and multiagent systems. He is a member of IEEE and SICE.

Iwanori Murakamireceived his Ph.D. Eng. from Gunma University in 1997. He is currently an associate professor at Gunma University. His research interests include robotics, applied electromagnetics and machines, and superconducting levitation applications.

Kou Yamada received B.S. and M.S. degrees in Electrical and Information Engineering from Yamagata University, Yamagata, Japan, 1987 and 1989, respectively; and the Dr. Eng. Degree from Osaka University, Osaka, Japan in 1997. Prof. Yamada is currently a full-time professor at Faculty of Science and Technology, Gunma University, Japan. His research interests include robust control, repetitive control, process control and control theory for inverse systems and infinite-dimensional systems. Prof. Yamada received the 2005 Yokoyama Award in Science and Technology, the 2005 Electrical Engineering/Electronics, Computer, Telecommunication, and Information Technology International Conference (ECTI-CON2005) Best Paper Award, the Japanese Ergonomics Society Encouragement Award for Academic Paper in 2007, the 2008 Electrical Engineering/Electronics, Computer, Telecommunication, and Information Technology International Conference (ECTI-CON2008) Best Paper Award and Fourth International Conference on Innovative Computing, Information and Control Best Paper Award in 2009, the 14th International Conference on Innovative Computing, Information and Control Best Paper Award in 2019, Outstanding Achievement Award from Kanto Branch of Japanese Society for Engineering Education in 2022, JSME (The Japan Society of Mechanical Engineers) Education Award in 2023 and the 2024 Electrical Engineering/Electronics, Computer, Telecommunication, and Information Technology International Conference (ECTI-CON2024) Best Paper Award. He is a member of IEEE and SICE and a Fellow of JSME.